CHEMISTRY
A EUROPEAN JOURNAL

DOI: 10.1002/chem.201100304

# Highly Efficient Blue Organic Light-Emitting Diodes Based on 2-(Diphenylamino)fluoren-7-ylvinylarene Derivatives that Bear a *tert*-Butyl Group

**Kum Hee Lee,[a] Young Soo Kwon,[a] Jin Yong Lee,[a] Sunwoo Kang,[a] Kyoung Soo Yook,[b] Soon Ok Jeon,[b] Jun Yeob Lee,*[b] and Seung Soo Yoon*[a]**

**Abstract:** Blue fluorescent materials with a 2-(diphenylamino)fluoren-7-ylvinylarene emitting unit and *tert*-butyl-based blocking units were synthesized. The photophysical properties of these materials, including UV/Vis absorption, photoluminescent properties, and HOMO–LUMO energy levels, were characterized and rationalized with quantum-mechanical DFT calculations. The electroluminescent properties of these molecules were examined through the fabrication of multilayer devices with a structure of indium–tin oxide, 4,4′-bis{*N*-[4-(*N,N*-di-*m*-tolylamino)phenyl]-*N*-phenylamino}biphenyl, 4′-bis[*N*-(1-naphthyl)-*N*-phenylamino]-biphenyl, and blue materials doped in 2-methyl-9,10-di(2-naphthyl)anthracene/tris(8-quinolinolato)aluminum/LiF/Al. All devices exhibit highly efficient blue electroluminescence with high external quantum efficiency (3.20–7.72 % at 20 mA cm$^{-2}$). A deep-blue device with Commission Internationale de l'Eclairage (CIE) coordinates of (0.15, 0.11) that uses 7-[2-(3′,5′-di-*tert*-butylbiphenyl-4-yl)vinyl]-9,9-diethyl-2-*N*-(3,5-di-*tert*-butylphenyl)-2,4-difluorobenzenamino-9*H*-fluorene as a dopant in the emitting layer showed a luminous efficiency and external quantum efficiency of 3.95 cd A$^{-1}$ and 4.23 % at 20 mA cm$^{-2}$, respectively. Furthermore, a highly efficient sky-blue device that uses the dopant 7-{2-[2-(3,5-di-*tert*-butylphenyl)-9,9′-spirobifluorene-7-yl]vinyl}-9,9-diethyl-2-*N,N*-diphenylamino-9*H*-fluorene exhibited a luminous efficiency and high quantum efficiency of 10.3 cd A$^{-1}$ and 7.7 % at 20 mA cm$^{-2}$, respectively, with CIE coordinates of (0.15, 0.20).

**Keywords:** density functional calculations · luminescence · organic light-emitting diodes · photophysics · quantum chemistry

## Introduction

In recent years, organic light-emitting diodes (OLEDs) have attracted considerable attention due to their potential applications in full-color, flat-panel displays and space illumination.[1,2] Red, green, and blue primary emitters are needed to produce full-color OLEDs for displays or lighting. High efficiency and saturated color have been achieved for red and green light-emitting materials.[3,4] However, blue devices require further improvement in their efficiency and color index. In particular, a highly efficient, pure deep-blue-emitting material needs to be developed to reduce OLED power consumption and increase the color range. Deep blue-emitting materials with a Commission Internationale de l'Eclairage *y* coordinate value (CIE *y*) of $<0.15$ are important not only for full-color displays, but also for solid-state lighting.[5]

However, it is difficult to design deep-blue-emitting materials with high efficiency, saturated color purity, and long operation times due to the wide bandgap of blue materials. Serious efforts to develop such materials have included host and dopant materials, such as diaryanthracenes,[6] di-(styryl)arylenes,[7] 4,4′-bis{2-[4-(*N,N*-diphenylamino)phenyl]-vinyl}biphenyl (BDAVBi),[8] and diphenylaminodi-(styryl)arylene (DSA-Ph).[9] Among the blue emitters developed thus far, an unsymmetrical mono(styryl)amine-based blue dopant known as BD-1 has high efficiency and a pure blue color.[10] A current efficiency of 5.4 cd A$^{-1}$ with CIE coordinates of (0.14, 0.13) and external quantum efficiency of 5.1 % were demonstrated by doping BD-1 in 2-methyl-9,10-di(2-naphthyl)anthracene (MADN). Unfortunately, blue dopant materials based on aromatic amine units suffer color-shifting problems at high doping concentrations due to intermolecular interactions between the dopant materials. Other than BD-1, few studies have reported deep-blue dopant materials with high efficiencies and a pure blue color.[11]

[a] Dr. K. H. Lee, Y. S. Kwon, Prof. J. Y. Lee, S. Kang, Prof. S. S. Yoon
Department of Chemistry, Sungkyunkwan University
300 Cheoncheon-dong, Jangan-gu, Suwon
Gyeonggi, 440-746 (Korea)
Fax: (+82) 31-290-7075
E-mail: ssyoon@skku.edu

[b] K. S. Yook, S. O. Jeon, Prof. J. Y. Lee
Department of Polymer Science and Engineering
Dankook University
126, Jukjeon-dong, Suji-gu, Yongin
Gyeonggi, 448-701 (Korea)
E-mail: leej17@dankook.ac.kr

Supporting information for this article is available on the WWW under http://dx.doi.org/10.1002/chem.201100304.

Fluorene moieties, such as alkylated fluorene, indenofluorene, and spirobifluorene, are expected to be good electroluminescent (EL) building units for OLED materials because fluorene-based core units have excellent fluorescent properties[12–15] as well as good morphological, thermal, and electrochemical stability.[15–19] Furthermore, fluorene moieties can be substituted easily with a range of functional groups,[20] and the fine-tuning of their EL properties though structural modification is relatively simple. However, only a few systematic studies have examined the EL properties of blue-emitting materials based on fluorene derivatives.

This paper reports the synthesis and electroluminescent properties of a series of newly designed, deep-blue-emitting materials based on 2-(diphenylamino)fluoren-7-ylvinylarene derivatives (**1**–**14**). In these materials, the diphenylaminofluorene core was combined with a vinylarene unit, thereby providing an extended conjugated structure to obtain a deep-blue color and enhanced light-emitting efficiency given the wide bandgap of the fluorene unit. The steric hindrance of the *tert*-butyl-based blocking group could prevent intermolecular interactions between the dopant materials and contribute to the high efficiency and deep-blue color, even at high doping concentrations.

Among the fourteen different blue materials studied, compound **1** had a 2-(diphenylamino)fluoren-7-ylstyrene emitting core without any blocking groups, whereas five other materials had the same emitting core with four different *tert*-butyl-substituted blocking groups: 3,5-di-*tert*-butylphenyl; 3,7-di-*tert*-butylnaphthyl; 2,7-di-*tert*-butyl-9,9-diethyl-4-fluorenyl; 4,4′-di-*tert*-butyl-2-biphenyl; and 3,5-bis(3′,5′-di-*tert*-butylphenyl)phenyl, which are shown here as compounds **2**, **3**, **4**, **5**, and **6**, respectively, to examine their effects on the device performance of blue fluorescent OLEDs. In addition, two different arenes, such as fluorene and spirobifluorene, between the 2-(diphenylamino)fluoren-7-ylvinyl moiety and 3,5-di-*tert*-butylphenyl blocking groups were introduced in blue fluorescent materials **7** and **8** to determine the substituent effect on the fluorophore. Furthermore, compounds **9**, **10**, and **11**, which were obtained by replacing diethylfluorene in compound **2** with spirobifluorene, diphenylfluorene, and spiroindanylfluorene, respectively, were studied to confirm the substituent effect on the 9,9-positions of the diphenylaminofluorene moiety. Finally, in compounds **12**, **13**, and **14**, fluorine with electron-withdrawing ability and a *tert*-butyl group with electron-donating ability were introduced to the diphenyl moiety to examine the electronic and steric effects on the EL performances of the devices using them. In this study, blue OLEDs with high efficiency, deep-blue color chromaticity, and stable CIE coordinates were developed using these novel blue materials based on the a 2-(diphenylamino)fluoren-7-ylvinylarene unit with a *tert*-butyl blocking group.

## Results and Discussion

**Synthesis and characterization**: Scheme 1 and Scheme 2 summarize the syntheses of the blue fluorescent materials (**1**–**14**). The blue-emitting materials (**1**, **2**, **4**, **5**, **6**, **7**, and **8**) were prepared in moderate yield by the Horner–Wadsworth–Emmons reaction between [7-(diphenylamino)-9,9-diethylfluorene-2-yl]methylphosphonate and the corresponding aldehyde compounds, such as **15**–**19**, which were synthesized from the Suzuki cross-coupling of 4-formylphenylboronic acid or 3,5-di-*tert*-butylphenylboronic ester, with the corresponding bromo intermediates. Compound **3** was prepared by Suzuki cross-coupling between 7-(diphenylamino)-2-(4-bromostyryl)-9,9-diethyl-9*H*-fluorene and 3,7-di-*tert*-bu-

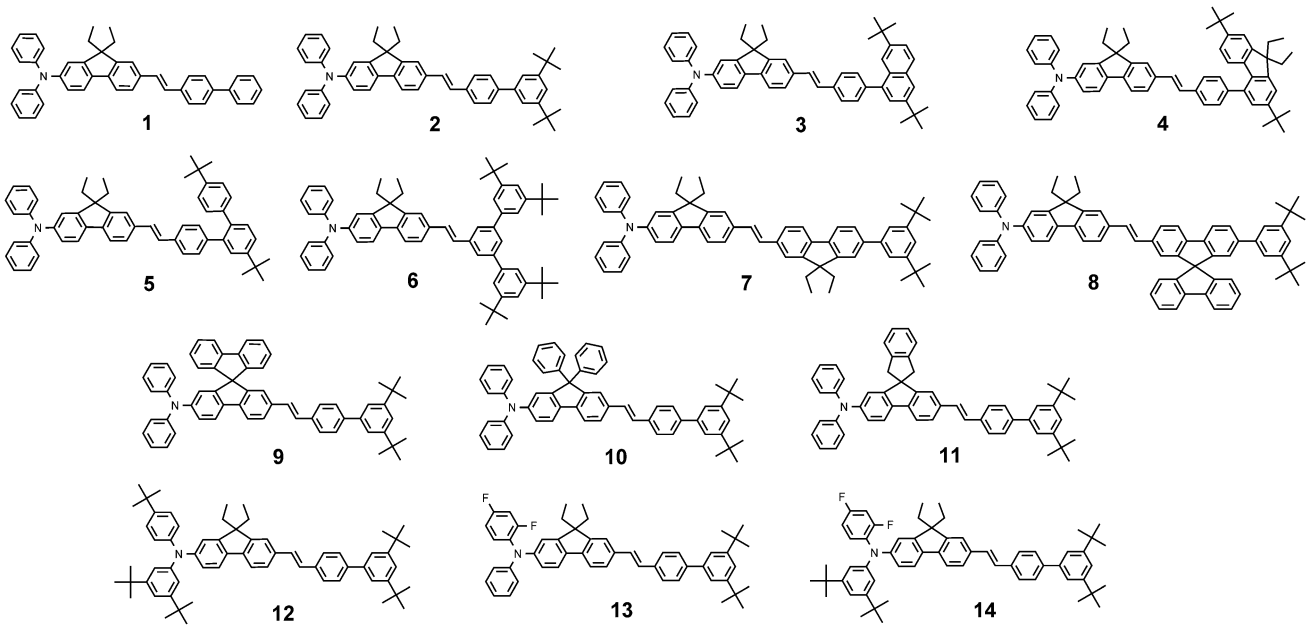


  

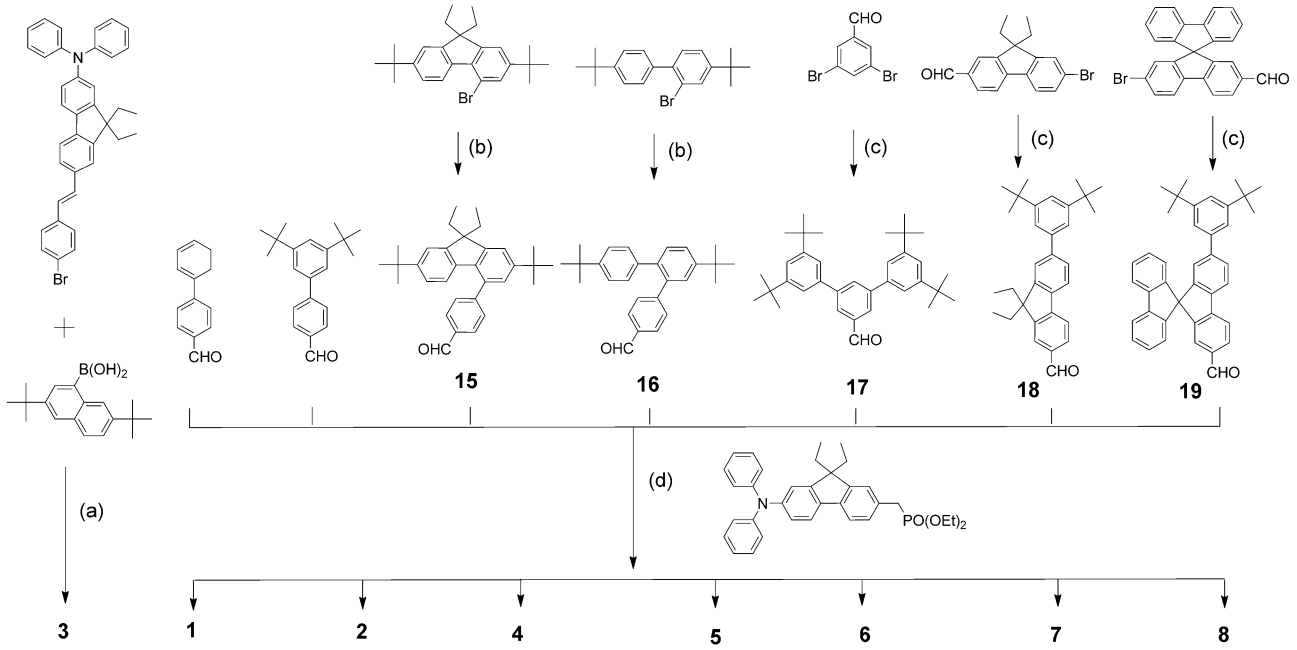


Scheme 1. The synthetic routes to blue fluorescent materials (**1**–**8**). Reagents: a) $[Pd(PPh_3)_4]/Na_2CO_3$/toluene/EtOH; b) 4-formylphenylboronic acid, $[Pd(PPh_3)_4]/Na_2CO_3$/toluene/EtOH; c) 2-(3,5-di-*tert*-butylphenyl)-4,4,5,5-tetramethyl-1,3,2-dioxaborolane, $[Pd(PPh_3)_4]/K_2CO_3$/toluene; and d) KO*t*Bu/THF.

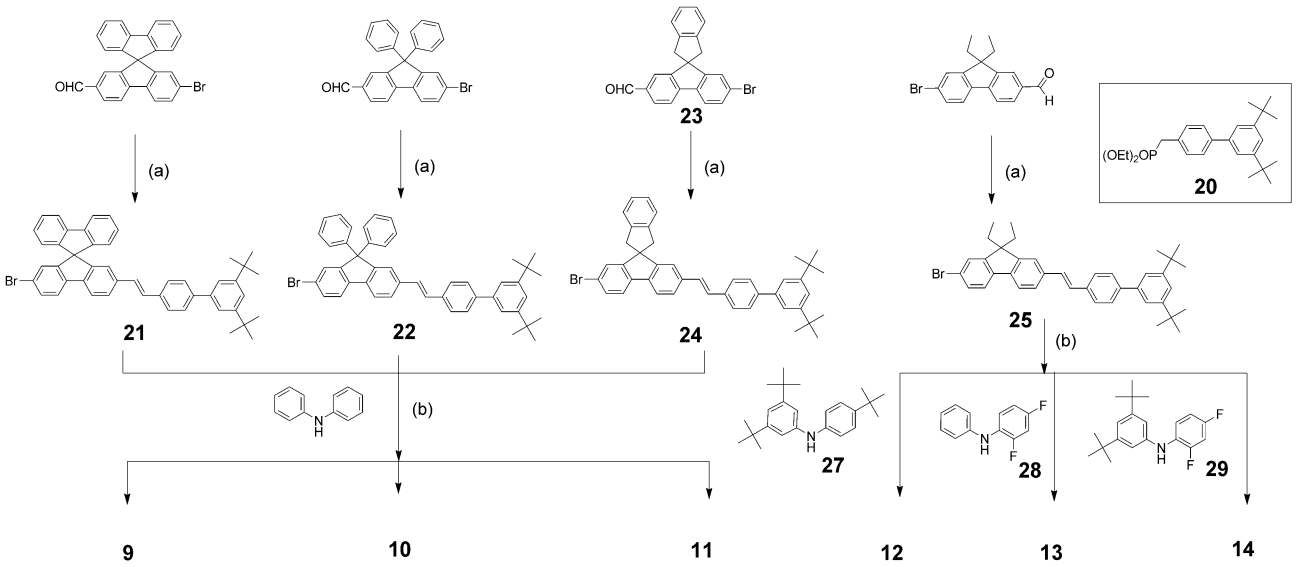


Scheme 2. The synthetic routes to blue fluorescent materials (**9**–**14**). Reagents: a) **20**, KO*t*Bu/THF; and b) $[Pd_2(dba)_3]$, $P(tBu)_3$, NaO*t*Bu, toluene.

tylnaphthalenyl-1-boronic acid. Compounds **9**, **10**, and **11** were prepared by synthetic routes consisting of the Horner–Wadsworth–Emmons reaction between diethyl (3′,5′-di-*tert*-butylbiphenyl)-4-methylphosphonate (**20**) and the corresponding aldehyde compounds, followed by Buchwald–Hartwig cross-coupling with diphenylamine.[21] Finally, Buchwald–Hartwig cross-coupling between 2-bromo-9,9-diethyl-7-[2-(3′,5′-di-*tert*-butylbiphenyl-4-yl)vinyl]-9*H*-fluorene (**25**) and the corresponding diarylamine (**26**, **27**, and **28**) afforded the blue-emitting materials (**12**, **13**, and **14**) in moderate yield. After the conventional purifications, such as column chromatography and recrystallization, these newly synthesized blue-emitting materials (**1**–**14**) were purified further by train sublimation under reduced pressure ($<10^{-3}$ torr) and fully characterized by $^1H$ and $^{13}C$ NMR spectroscopy, infrared (IR), elemental analysis, and low- and high-resolution mass spectrometry. High-pressure liquid chromatography (HPLC) was carried out to examine the purity of materials. These analyses revealed that the blue-emitting materials (**1**–**14**) is at least >99.0% pure.

  

**Photophysical properties**: The UV/Vis absorption and photoluminescence (PL) spectra of the synthesized blue materials were obtained in dichloromethane (Figure 1). Compounds **1**–**6**, **9**, **10**, and **12** showed similar UV/Vis spectra, regardless of blocking groups and substituents on the 9,9-positions of the diphenylaminofluorene moiety. These observations suggest that the substituents did not have a significant effect on the UV/Vis absorption; UV/Vis light was absorbed mostly by the 2-diphenylaminofluorene-7-ylstyrene core units. The edge of the UV/Vis spectra of these dopant materials, which was used to calculate the bandgap, revealed a similar bandgap of around 2.90 eV in materials **1**–**6**, **9**, **10**, and **12**, even though small substituent-dependent differences were observed. Compared to compound **2**, the maximum peaks of the UV/Vis absorption spectra of compounds **7** and **8** were observed at 397 and 398 nm on account of the extended π-conjugation length of the chromophores. Compared to compound **2** with only hydrogen atoms on the diphenyl moiety, the maximum peak of the UV/Vis absorption spectrum of compound **12** with three electron-donating *tert*-butyl units was redshifted by 10 nm, whereas that of compound **13** with two electron-withdrawing fluorine atoms exhibited a blueshift of 6 nm. Interestingly, compound **14** with both electron-donating *tert*-butyl units and electron-withdrawing fluorine atoms on the diphenyl moiety showed a similar maximum peak of the UV/Vis absorption spectrum to compound **12**. As will be seen below in the quantum-mechanical calculation section, the electron densities of HOMO in the blue materials (**1**–**14**) are concentrated on diphenylamine moieties, whereas those of LUMO are spread over the other moiety of materials. Therefore, the electron-donating or -withdrawing groups on the phenyl group of the diphenylamine moiety would affect the energy levels of the HOMO more significantly than the LUMO of this type of material. Therefore, electron-donating groups on compound **12** decrease the energy bandgap by the increasing HOMO energy level of compound **12**, and thus induce a redshift in the UV/Vis absorption spectrum compared to compound **2**, whereas the electron-withdrawing groups on compound **13** increase the energy bandgap by lowering HOMO energy level of compound **13** and inducing a blueshift in the UV/Vis absorption spectrum relative to compound **2**. In compound **14**, the effects of the electron-donating and -withdrawing groups are cancelled out, and its UV/Vis absorption spectrum is similar to that of compound **2**. The UV/Vis absorption spectra of blue materials (**1**–**14**) overlapped well with the PL emission spectra of a common blue host, MADN. This suggests that energy transfer between MADN and these materials is quite efficient and MADN is a good host in OLED devices using these materials as dopants.

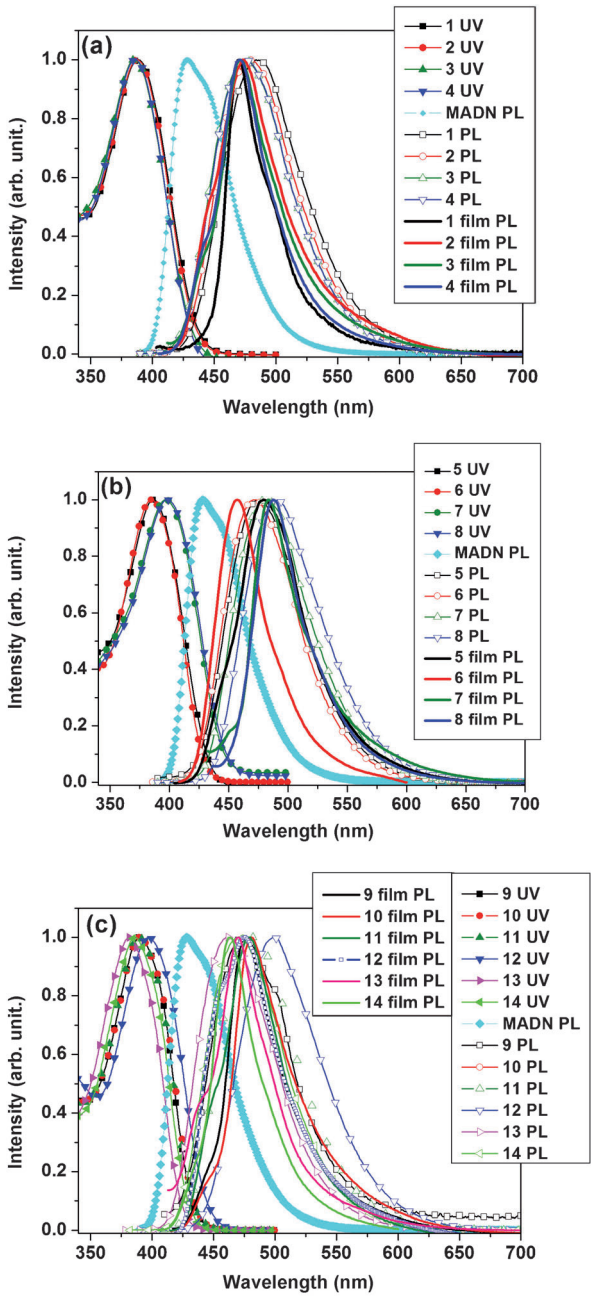


Figure 1. UV and PL spectra of blue fluorescent materials (**1**–**14**).

The maximum peaks of the PL spectra of compounds **2**–**5** were 476 nm, whereas that of compound **1**, without any blocking groups, had a maximum peak of 478 nm. The redshift of the emission peaks was attributed to the extended conjugation structure of compound **1**, as shown below in the molecular calculation. Interestingly, compound **6** showed a hypsochromic shift in the emission peak of 4 nm relative to the PL spectrum of compound **2** due to the shortening of the π-conjugation length by *meta* substitution, not *para* substitution, of 3,5-di-*tert*-butylbenzene. In the case of compounds **12**, **13**, and **14**, the PL spectra showed similar trends to the UV/Vis absorption spectra. Therefore, in compound **12**, a redshift of 24 nm occurred when the *tert*-butyl group was added to the diphenyl moiety of compound **2**. In contrast, compound **13** exhibited hypsochromic shift (14 nm) relative to compound **2** due to the increased electron-withdrawing effect by the fluorine atoms. In addition, the PL spectrum of compound **14** is similar to that of compound **2**. The PL quantum yield of materials (**1**–**14**) were measured to

  

have a quantum yield >0.60, thereby indicating that the diphenylaminofluorene-based core was an efficient emitting unit, and thus high efficiency could be expected in a blue device that used these materials. Figure 1 shows the PL spectra of the blue materials (**1**–**14**) in thin solid film on quartz plates. All the blue materials (**1**–**14**) showed a narrower full width at half-maximum (fwhm; 10–41 nm) in the film than in solution. The narrower emission bands in the films suggest that these materials could have improved color purity in solid-state OLED devices. Table 1 lists the basic physical properties of these materials.

Table 1. Physical properties of the compounds **1**–**14**.

| Dopants | UV $\lambda_{max}$ [nm][a] | PL $\lambda_{max}$ [nm][a,b] | fwhm [nm][a,b] | HOMO | LUMO | $E_g$ | $\Phi$[c] |
|---|---|---|---|---|---|---|---|
| **1** | 388 | 478/470 | 76/35 | −5.43 | −2.54 | 2.89 | 0.95 |
| **2** | 388 | 476/473 | 74/64 | −5.45 | −2.55 | 2.90 | 0.94 |
| **3** | 386 | 476/471 | 74/52 | −5.55 | −2.62 | 2.93 | 0.97 |
| **4** | 386 | 476/471 | 73/49 | −5.47 | −2.55 | 2.92 | 0.91 |
| **5** | 386 | 476/480 | 73/65 | −5.57 | −2.64 | 2.93 | 0.97 |
| **6** | 385 | 472/457 | 71/50 | −5.59 | −2.67 | 2.92 | 0.82 |
| **7** | 397 | 482/484 | 74/50 | −5.44 | −2.61 | 2.83 | 0.81 |
| **8** | 398 | 492/488 | 76/50 | −5.47 | −2.66 | 2.81 | 0.97 |
| **9** | 390 | 474/476 | 77/48 | −5.53 | −2.62 | 2.91 | 0.86 |
| **10** | 390 | 477/480 | 72/52 | −5.51 | −2.63 | 2.88 | 0.99 |
| **11** | 390 | 482/480 | 75/56 | −5.50 | −2.63 | 2.87 | 0.95 |
| **12** | 398 | 500/476 | 77/66 | −5.29 | −2.48 | 2.81 | 0.79 |
| **13** | 382 | 462/470 | 73/52 | −5.70 | −2.75 | 2.95 | 0.62 |
| **14** | 386 | 470/464 | 73/53 | −5.63 | −2.72 | 2.91 | 0.62 |

[a] In $CH_2Cl_2$ ($\approx 1\times10^{-5}$ M). [b] In neat film. [c] Quantum yield using BDAVBi as a standard; $\lambda_{ex}=360$ nm ($\Phi=0.86$ in $CH_2Cl_2$).

**Measurement of the energy levels of the materials**: The HOMO energy levels of these materials were estimated using an AC-2 photoelectron spectrometer to show that the HOMO energy levels of compounds **1**–**11** varied from −5.43 to −5.59 eV, respectively (Table 1). The LUMO energy levels, which were calculated by subtracting the optical bandgaps from the HOMO energy levels, ranged from −2.54 and −2.66 eV. The energy bandgap of the blue fluorescent materials (**1**–**14**) ranged from 2.81 to 2.95 eV, which are narrower than the 3.0 eV for MADN, thereby demonstrating the suitability of compounds **1**–**14** and MADN to act as dopants and hosts, respectively, in blue OLEDs. Interestingly, when the electron-donating *tert*-butyl groups were added to the diphenylaminofluorene group of compound **12**, the energy bandgap became 2.81 eV, which is 0.09 eV narrower than that of compound **2**. In addition, compared to the energy bandgap of compound **2** (2.90 eV), the energy bandgap of **13** became 2.95 eV when electron-withdrawing fluorine atoms were added to the diphenylaminofluorene group of compound **13**. The energy bandgap of compound **14** (2.91 eV) is similar to that of compound **2**. These results are in good agreement with the trends observed in the absorption and emission spectra, and the quantum mechanical calculations. Figure 2 shows the HOMO and LUMO energy levels of blue fluorescent materials (**1**–**14**), along with the other materials employed here in electroluminescent devices, including indium–tin oxide (ITO); 4,4′-bis{*N*-[4-(*N*,*N*-di-*m*-tolylamino)phenyl]-*N*-phenylamino}biphenyl (DNTPD); 4′-bis[*N*-(1-naphthyl)-*N*-phenylamino]biphenyl (NPB); MADN; tris(8-quinolinolato)aluminum ($Alq_3$); and LiF:Al.

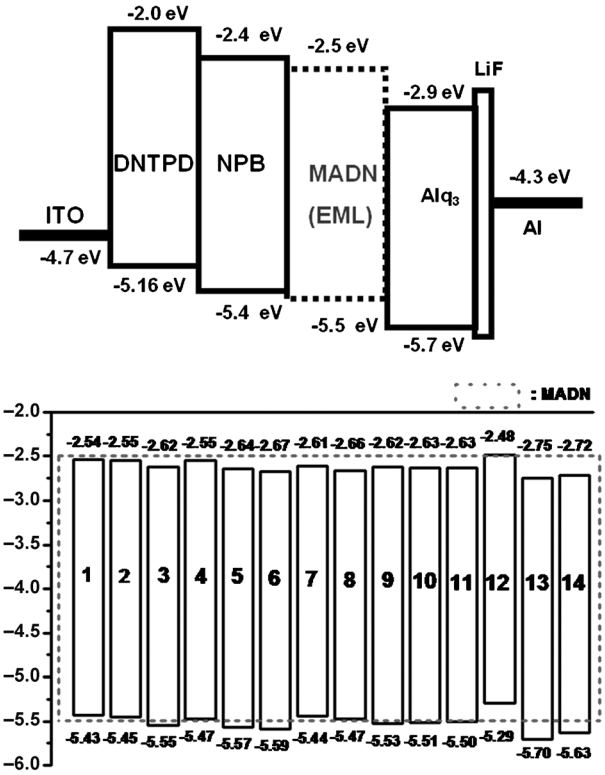


Figure 2. Energy-level diagram of the materials used in the devices.

**Quantum-mechanical calculation of electronic structures**: To better understand the observed photophysical properties of the organic light-emitting diode materials at the molecular level, density functional theory (DFT) calculations for compounds **1**–**14** were carried out using the nonlocal density functional of Becke's three parameters and employing the Lee–Yang–Parr functional (B3LYP) with 6-31G* basis sets using a suite of Gaussian 03 programs.[22] The calculations showed that the dihedral angles between the fluorene (linked with diphenyl amine or substituted diphenyl amine moiety) and benzene (linked with styryl) moieties were 9.18, 7.89, 7.33, 9.33, 6.54, 3.89, 3.43, 0.30, 3.14, 1.02, 0.82, and 1.58° for compounds **1**–**6** and **9**–**14**, respectively. For compounds **7** and **8**, the calculated dihedral angles between the fluorene (linked with diphenyl amine) and fluorene (spirofluorene) were 1.68 and 0.61°, respectively. The calculated dihedral angles between benzene (linked with styryl) and substituents for compounds **1**–**6** and **9**–**14** were 36.7, 37.9, 53.8, 58.7, 50.5, 39.9, 37.2, 37.6, 37.0, 37.4, 37.7, and 37.9°, respectively. For compounds **7** and **8**, the calculated dihedral angles between fluorene (spirofluorene) and the substituents were 37.9 and 37.4°, respectively, and the substituents of all of the compounds were out of plane. Figure 3 presents the HOMOs and LUMOs for compounds **1**–**14**. The shapes of

  

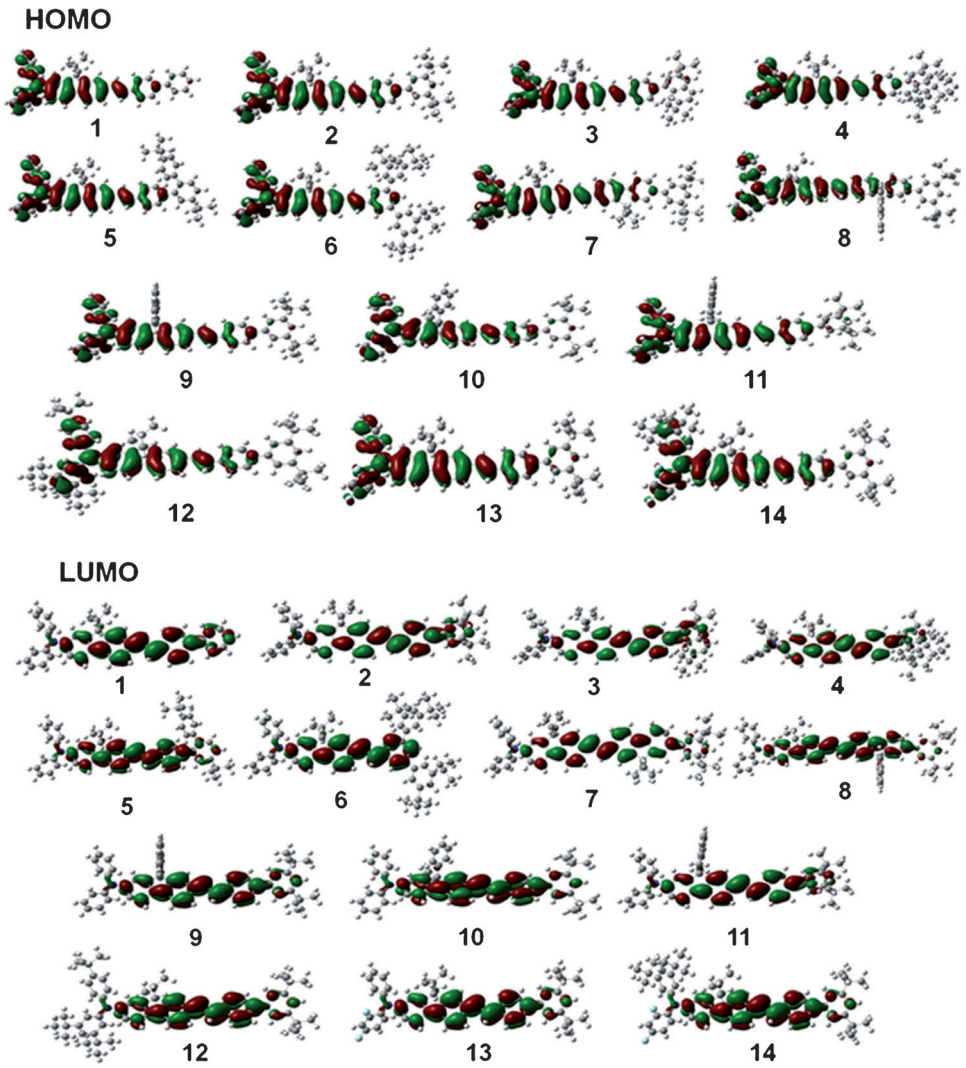


Figure 3. B3LYP/6-31G*-calculated HOMOs and LUMOs orbitals of blue fluorescent materials (**1**–**14**).

the HOMOs and LUMOs for all the compounds appear similar. In the HOMOs of compounds **1**–**6** and **9**–**14**, the electrons are distributed over the 2-diphenylaminofluoren (spirofluoren, diphenylfluoren, indanylfluoren)-7-ylstyrene moiety, whereas in the LUMOs, they are distributed over the fluoren-7-ylvinylarene moieties. For compounds **7** and **8**, the HOMO electrons are distributed over the 2-diphenylaminofluoren-7-ylfluorene and 2-diphenylaminofluoren-7-ylspirobifluorene moieties, respectively, whereas the LUMO electrons are distributed over the fluoren-7-ylvinylarenes. The electrons in the HOMOs for compounds **13** and **14** are distributed over the 2-*N*-2,4-difluorophenyl-*N*-phenylamino-7-ylstyrene moiety and 2-*N*-2,4-difluorophenyl-*N*-3,5-di-*tert*-butylphenylaminofluoren-7-ylstyrene moiety, whereas the electrons in the LUMOs are distributed over the fluoren-7-ylvinylarene moieties.

Time-dependent DFT (TD-DFT) calculations were carried out at the optimized geometries to investigate the electronic transition energies and properties. The HOMO→LUMO transition contributes solely to the excitations for compounds **1**–**14**; the results are listed in Table 2. The excitation energies calculated for compounds **1**–**6** are 2.8715, 2.8890, 2.8799, 2.9022, 2.9024, and 2.9523 eV, respectively, which correspond to the absorption wavelengths of 431.78, 429.16, 430.52, 427.21, 427.18, and 419.96 nm, respectively. The calculated HOMO–LUMO gaps for compounds **2**–**6** are larger than that of compound **1** because the LUMO for compound **1** shows more delocalization than compounds **2**–**6**. In other words, the energy level of the LUMO for compounds **2**–**6** is higher than that of compound **1**, thereby resulting in large HOMO–LUMO gap values. The HOMO–LUMO gaps of compounds **7** and **8** are smaller than those of compounds **1**–**5** because the lengths of the chromophores of compounds **7** and **8** are longer than those of compounds **1**–**5**. The HOMO–LUMO gaps of compounds **7** and **8** are 2.7988 and 2.7832 eV, respectively, which correspond to absorption wavelengths of 443.0 and 445.47 nm. The HOMO–LUMO gaps of compounds **9**–**11** are 2.8780, 2.8703, and 2.8808 eV, which correspond to the absorption wavelengths of 430.80, 431.96, and 430.39 nm, respectively. For

Table 2. Oscillation strength and electronic transition for compounds **1**–**14**.

| Compound | Oscillation strength | Transition ([%]) | $\lambda_{abs,max}$ [nm][a] | $\lambda_{abs,max}$ [nm][b] |
|---|---|---|---|---|
| **1** | 1.3833 | HOMO to LUMO (100) | 431.78 | 388 |
| **2** | 1.4986 | HOMO to LUMO (100) | 429.16 | 388 |
| **3** | 1.4781 | HOMO to LUMO (100) | 430.52 | 386 |
| **4** | 1.4547 | HOMO to LUMO (100) | 427.21 | 386 |
| **5** | 1.4245 | HOMO to LUMO (100) | 427.18 | 386 |
| **6** | 1.2833 | HOMO to LUMO (100) | 419.96 | 385 |
| **7** | 1.9494 | HOMO to LUMO (100) | 443.00 | 397 |
| **8** | 1.9070 | HOMO to LUMO (100) | 445.47 | 398 |
| **9** | 1.4867 | HOMO to LUMO (100) | 430.80 | 390 |
| **10** | 1.4494 | HOMO to LUMO (100) | 431.96 | 390 |
| **11** | 1.5151 | HOMO to LUMO (100) | 430.39 | 390 |
| **12** | 1.4412 | HOMO to LUMO (100) | 440.84 | 398 |
| **13** | 1.6363 | HOMO to LUMO (100) | 420.38 | 382 |
| **14** | 1.5687 | HOMO to LUMO (100) | 426.81 | 386 |

[a] Calculated absorption wavelength. [b] Measured absorption wavelength.

  

compounds **12**–**14**, the calculated HOMO–LUMO gaps are 2.8125, 2.9493, and 2.9049 eV, respectively, which correspond to the absorption wavelengths of 440.84, 420.38, and 426.81 nm, respectively. The absorption wavelengths of compounds **12**–**14** are shifted by 10.68, −8.78, and −2.35 nm, respectively, relative to compound **2**. In compound **12**, electron-donating *tert*-butyl groups are substituted in the high-electron-density moiety (biphenyl amino moiety) of the HOMO. Hence, the HOMO–LUMO gap is narrower than that of compound **2** due to the growth of the HOMO energy level. In the case of compound **13**, fluorine substituent lowers the energy level of HOMO and increases the HOMO–LUMO gap. For compound **14**, the electron-donating *tert*-butyl substituent leads to an increase in the HOMO energy level, whereas the fluorine atom extracts the electron density and lowers the energy level of the HOMO. Therefore, HOMO–LUMO gap of compounds **14** and **2** are similar. These results are in good agreement with the experimentally observed absorption wavelengths.

**Electroluminescence properties**: The device performance of the blue fluorescent materials (**1**–**14**) was examined by doping these materials in the MADN host at a 5–15% concentration, with the following device structure: ITO/DNTPD (60 nm)/NPB (30 nm)/**1**–**14** doped in MADN (30 nm)/$Alq_3$ (20 nm)/LiF (1.0 nm)/Al (200 nm). Table 3 summarizes the device performances, and Figure 4 presents the EL spectra of the blue device with a 5% doping concentration (**1A**–**14A**). All devices exhibited blue emission with emission peaks between 441 and 484 nm. The contribution of the host MADN to the electroluminescence (EL) emission can be excluded because of the superior EL performance of devices **1A**–**14A** relative to that of a similar device using only MADN as the emitting layer. This suggests that the EL emission of devices **1A**–**14A** originates from the emissions of dopants **1**–**14** through Forster-type energy transfer between the dopants and MADN host. With the exception of devices **7A**, **8A**, and **12A**, which have a wider energy bandgap than the others, eleven devices **A** showed deep-blue colors with a *y* CIE coordinate $<0.16$ due to the blue-emitting diphenylaminofluorene-7-ylstyrene core unit. However, the CIEs of the devices were dependent on the blocking groups of the dopant materials. For example, device **1A** that used compound **1** without a blocking group as a dopant showed a *y* CIE of 0.16, whereas devices **A** that used dopant materials **2**–**6**, **9**–**11**, **13**, and **14** with *tert*-butyl-based blocking groups showed a *y* coordinate of $<0.15$, thus indicating a blueshift in the CIE color coordinates of the devices due to the introduction of a blocking group on the dopants. These blueshifts could be explained by the protection of the

Table 3. EL performance characteristics of devices **1**–**14**.

| Devices | Dopants [(wt%)] | $\eta_L$[a] | $\eta_P$[b] | $\eta_{ext}$[c] | $L$[d] | $V_{on}$[e] | EL[f] | CIE ($x$, $y$)[f] |
|---|---|---|---|---|---|---|---|---|
| MADN only | | 2.4 | 1.28 | 1.96 | 160 | 6.0 | 462 | (0.15, 0.16) |
| **1A** | **1** (5) | 6.28 | 3.11 | 5.27 | 4081 | 5.0 | 455, 474 | (0.15, 0.16) |
| **1B** | **1** (10) | 6.31 | 3.03 | 4.92 | 3102 | 5.0 | 457, 477 | (0.15, 0.18) |
| **1C** | **1** (15) | 5.75 | 3.00 | 4.31 | 5617 | 4.5 | 458, 478 | (0.15, 0.19) |
| **2A** | **2** (5) | 5.42 | 3.10 | 5.17 | 10200 | 4.5 | 451 | (0.15, 0.13) |
| **2B** | **2** (10) | 5.07 | 2.84 | 4.47 | 7623 | 4.5 | 452, 472 | (0.15, 0.14) |
| **2C** | **2** (15) | 4.85 | 2.81 | 4.14 | 9502 | 4.5 | 453, 472 | (0.15, 0.15) |
| **3A** | **3** (5) | 4.09 | 2.17 | 3.96 | 4847 | 5.0 | 450 | (0.15, 0.13) |
| **3B** | **3** (10) | 4.12 | 2.19 | 3.82 | 4852 | 5.0 | 451 | (0.15,0.14) |
| **3C** | **3** (15) | 3.01 | 1.76 | 2.84 | 5430 | 5.0 | 453 | (0.15,0.17) |
| **4A** | **4** (5) | 3.81 | 2.11 | 3.39 | 5151 | 4.0 | 450 | (0.15, 0.14) |
| **4B** | **4** (10) | 4.21 | 2.39 | 3.58 | 6903 | 4.5 | 452, 472 | (0.14, 0.15) |
| **4C** | **4** (15) | 4.42 | 2.43 | 3.81 | 5346 | 4.5 | 454, 472 | (0.14, 0.15) |
| **5A** | **5** (5) | 4.18 | 2.18 | 4.13 | 3406 | 5.0 | 449 | (0.15, 0.13) |
| **5B** | **5** (10) | 3.41 | 1.71 | 3.37 | 1652 | 5.0 | 449 | (0.15,0.13) |
| **5C** | **5** (15) | 2.54 | 1.35 | 2.25 | 1167 | 5.0 | 450 | (0.15,0.14) |
| **6A** | **6** (5) | 3.82 | 2.13 | 3.89 | 3543 | 5.0 | 447 | (0.15, 0.12) |
| **6B** | **6** (10) | 4.06 | 2.17 | 3.86 | 5155 | 4.5 | 448, 461 | (0.15, 0.13) |
| **6C** | **6** (15) | 3.69 | 1.97 | 3.60 | 4648 | 5.0 | 447, 463 | (0.15, 0.15) |
| **7A** | **7** (5) | 8.44 | 4.67 | 6.83 | 13550 | 4.5 | 456 | (0.15, 0.17) |
| **7B** | **7** (10) | 8.58 | 4.27 | 5.48 | 14860 | 4.5 | 458 | (0.15,0.19) |
| **7C** | **7** (15) | 7.55 | 4.02 | 4.56 | 14790 | 4.5 | 459 | (0.15,0.20) |
| **8A** | **8** (5) | 10.3 | 5.11 | 7.67 | 5651 | 5.5 | 458, 482 | (0.15, 0.20) |
| **8B** | **8** (10) | 10.9 | 5.42 | 7.72 | 5750 | 5.5 | 460, 484 | (0.15, 0.20) |
| **8C** | **8** (15) | 10.5 | 5.23 | 7.27 | 6512 | 5.5 | 461, 484 | (0.15, 0.21) |
| **9A** | **9** (5) | 5.85 | 2.90 | 4.97 | 4477 | 5.0 | 449, 472 | (0.15, 0.15) |
| **9B** | **9** (10) | 6.61 | 3.17 | 5.43 | 4029 | 5.0 | 450, 473 | (0.15,0.16) |
| **9C** | **9** (15) | 6.20 | 3.20 | 4.91 | 5185 | 5.0 | 451, 474 | (0.15,0.17) |
| **10A** | **10** (5) | 4.79 | 2.56 | 4.21 | 6849 | 4.5 | 449, 472 | (0.15, 0.14) |
| **10B** | **10** (10) | 5.40 | 2.89 | 4.68 | 6604 | 4.5 | 449, 473 | (0.15, 0.15) |
| **10C** | **10** (15) | 6.25 | 3.34 | 5.35 | 11440 | 4.5 | 449, 473 | (0.15, 0.15) |
| **11A** | **11** (5) | 6.12 | 3.27 | 5.41 | 7341 | 4.5 | 451, 473 | (0.15, 0.15) |
| **11B** | **11** (10) | 6.38 | 3.48 | 5.12 | 9536 | 4.5 | 453, 476 | (0.15, 0.17) |
| **11C** | **11** (15) | 6.24 | 3.61 | 5.08 | 17190 | 4.5 | 454, 476 | (0.14, 0.16) |
| **12A** | **12** (5) | 6.24 | 3.54 | 4.97 | 14350 | 4.5 | 456, 481 | (0.14, 0.17) |
| **12B** | **12** (10) | 6.84 | 3.96 | 5.00 | 17670 | 4.0 | 457, 481 | (0.14, 0.19) |
| **12C** | **12** (15) | 6.85 | 3.81 | 5.14 | 27280 | 4.0 | 457, 481 | (0.14, 0.19) |
| **13A** | **13** (5) | 3.54 | 1.54 | 3.20 | 612.7 | 6.0 | 443, 463 | (0.15, 0.15) |
| **13B** | **13** (10) | 4.16 | 1.71 | 3.56 | 451.2 | 6.0 | 443, 464 | (0.15,0.16) |
| **13C** | **13** (15) | 4.26 | 1.76 | 3.55 | 459.1 | 6.0 | 443, 465 | (0.15,0.17) |
| **14A** | **14** (5) | 3.95 | 1.96 | 4.23 | 3299 | 6.0 | 443, 462 | (0.15, 0.11) |
| **14B** | **14** (10) | 4.50 | 2.32 | 4.53 | 4004 | 5.0 | 444, 465 | (0.15, 0.13) |
| **14C** | **14** (15) | 4.07 | 2.18 | 3.98 | 4713 | 4.5 | 444, 466 | (0.15, 0.13) |

[a] Luminous efficiency [$cd\,A^{-1}$] at 20 $mA\,cm^{-2}$. [b] Power efficiency [$lm\,W^{-1}$] at 20 $mA\,cm^{-2}$. [c] External quantum efficiency [%] at 20 $mA\,cm^{-2}$. [d] Luminance [$cd\,m^{-2}$] at 8 V. [e] Turn-on voltage at 1 $cd\,m^{-2}$. [f] CIE $x$, $y$ coordinates at 8.0 V.

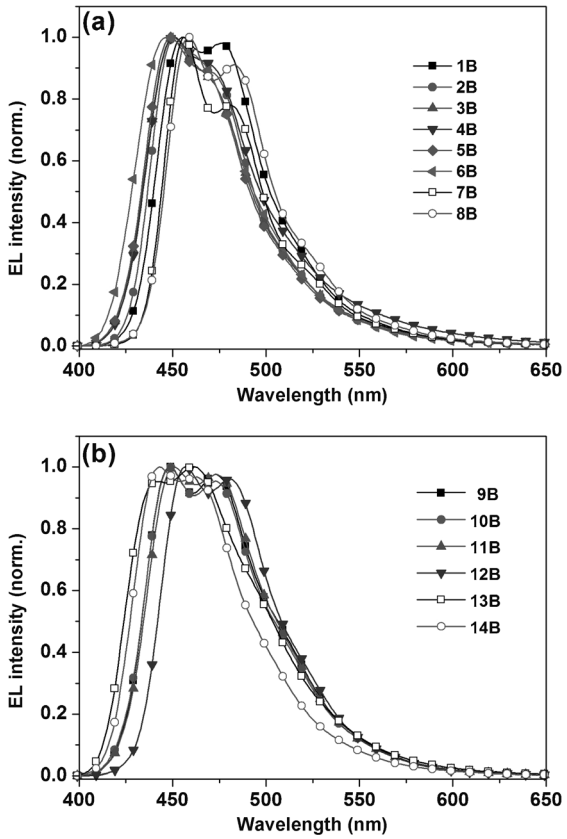


Figure 4. EL spectra of blue OLEDs (**1A**–**14A**) at 8 V.

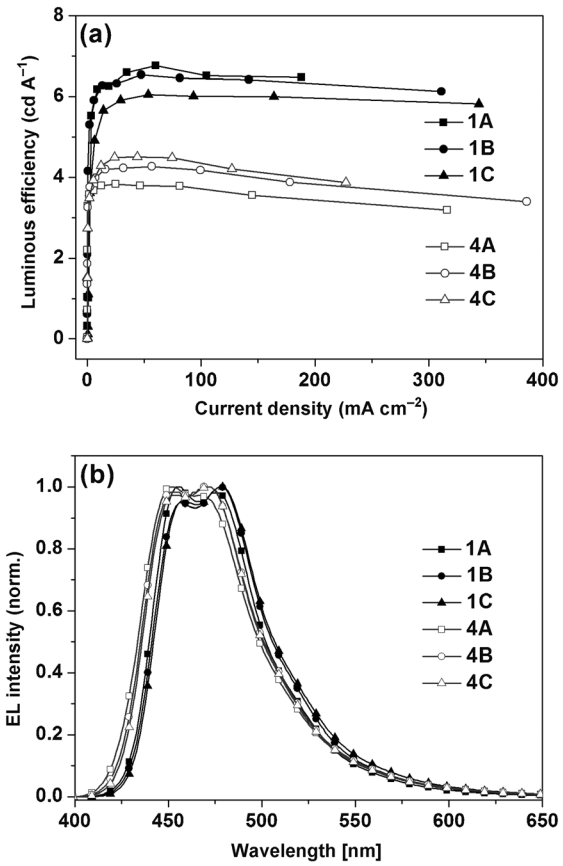


Figure 5. a) Comparison of the current efficiency of devices using **1** and **4** depending on doping concentration. b) EL spectra of the devices using **1** and **4** depending on doping concentration

emitting core of the dopants by the bulky *tert*-butyl-based blocking groups, which suppressed the intermolecular interactions between the dopant materials. The reduced interactions led to a blueshift in the emission peaks observed in the EL spectra of the devices that used them as dopants (Figure 4). Among devices **1A**–**14A**, device **14A**, which used compound **14** as a dopant, showed the best CIE coordinates of (0.15, 0.11). In addition, the compound **6**-doped device **6A** exhibited deep-blue emission with CIE coordinates of (0.15, 0.12).

The effects of the *tert*-butyl-based blocking group was confirmed by an examination of the performance of the devices built using compounds **1** and **4** in terms of their doping concentrations, as shown in Table 3 and Figure 5a. In general, the external quantum efficiency (EQE) of the blue fluorescent materials decreases at high doping concentrations due to concentration-quenching effects with the optimum doping being observed at approximately 5% in most cases.[23] A similar result was obtained in devices that used compound **1** as a dopant, in which the quantum yield decreased with increasing doping concentration. The EQEs of the compound **1** doped devices at 5 and 15% concentrations were 5.3 and 4.2%, respectively. However, the efficiency of the devices that used compound **4** as a dopant improved at high doping concentrations. The EQEs of the compound **4** doped devices at 5 and 15% concentrations were 3.4 and 3.8%, respectively, and showed >10% improvement at higher doping concentrations. The improved EQE of the devices that used compound **4** as a dopant at higher doping concentrations suggests that the hydrocarbon-based, nonpolar blocking groups of compound **4** reduces the level of molecular aggregation in the emitting layer and suppresses self-quenching, even at concentrations as high as 15%. The EL spectra of the devices that used compounds **1** and **4** as dopants support this notion, as shown in Figure 5b. In devices that used compound **4** as a dopant, there was little change in the EL spectra with various doping concentrations, but the spectral intensity between 480 and 700 nm was higher in the devices that used compound **1** as a dopant at higher concentrations. This increased EL emission peak intensity was attributed to intermolecular interactions of the dopant materials. The CIE coordinates of devices **4** were (0.15, 0.14) and (0.14, 0.15) at a 5 and 15% doping concentration, respectively, whereas the CIE of devices **1** were (0.15, 0.16) and (0.15, 0.19) at a 5 and 15% doping concentration, respectively. Therefore, the *tert*-butyl-based blocking group is effective in keeping the EL spectra constant at longer wavelengths, irrespective of the doping concentration, and in allowing high efficiency even at high concentrations.

Interestingly, in the devices that used compound **2** as a dopant, *tert*-butyl-based blocking groups, such as 3,5-di-*tert*-

  

butylbenzene, do not play an important role in the EL efficiency because the EL efficiencies of the devices that used compounds **1** and **2** as a dopant were similar (Figure 6). This suggests that in contrast to 2,7-di-*tert*-butyl-9,9-diethyl-4-fluorenyl group of compound **4**, the 3,5-di-*tert*-butylbenzene group of compound **2** is not bulky enough to affect molecular aggregation and EL efficiencies of the devices that used compound **2** as a dopant. Interestingly, the devices that used compounds **6**, **10**, **11**, **12**, and **14** as dopants exhibited the effects of a *tert*-butyl-based blocking group on the EL efficiencies. In particular, the EQEs of the compound **10** doped devices at 5 and 15% concentrations were 4.2 and 5.4%, respectively, and showed a 29% improvement at higher doping concentrations. In addition, the EQEs of the devices that used compounds **6**, **11**, **12**, and **14** as dopants at 5 and 15% concentrations were in a similar range within 7.5%, respectively, whereas the EQEs of the device that used compound **2** as a dopant at a 15% concentration decreased by 20% relative to that at a 5% concentration. This suggests that the introduction of additional groups to compound **2** would increase the molecular size of compounds **6**, **10**, **11**, **12**, and **14** and reduce the level of molecular aggregation in the emitting layer of the devices that used them as dopants, even at concentrations as high as 15%, as shown in devices that used compound **4** as a dopant.

The EL efficiencies of devices show complex correlations with the molecular structure of the blue dopants in the emitting layer. First of all, a change of the *tert*-butyl blocking group from the 3,5-di-*tert*-butylphenyl group to the 3,7-di-*tert*-butylnaphthyl group, 2,7-di-*tert*-butyl-9,9-diethyl-4-fluorenyl group, 4,4′-di-*tert*-butyl-2-biphenyl group, and the 3,5-bis(3′,5′-di-*tert*-butylphenyl)phenyl group decreased the EQE by 30, 52, 25, and 33% (**2B** versus **3B**, **4B**, **5B**, and **6B**), respectively. In addition, the substitution of diethyl groups at the 9,9 positions of the fluorene moiety of dopant **2** to diphenyl groups, spirodiphenyl groups and spiroindanyl influenced the EL efficiency of the devices that used them as dopants (**2B** versus **9B**, **10B**, and **11B**). For example, relative to device **2B**, the EQEs of devices **9B** and **10B** decreased by 3.9 and 19%, respectively, whereas the EQE of device **11B** increased by 4.6%. Furthermore, the additional *tert*-butyl groups and fluorine atoms in the diphenylamine moiety of compound **2** significantly altered the EL efficiency of the devices. For example, relative to device **2B**, devices **12B**, **13B**, and **14B** showed a 3.9, 38, and 18% decrease in the EQE, respectively. These observations reflect the complex aspects of the host–dopant system in the emitting layer of the OLED devices.

Among devices **1A**–**14A**, devices **7A** and **8A** showed the highest EQE, whereas the CIE coordinates of devices **7A** and **8A** indicated a redshift (0.04 and 0.07) from that of device **2A** in the CIE *y* coordinate due to an extension of the π-conjugation length by fluorene and spirobifluorene. The best luminous efficiency and EQE were achieved in device **8A**, with 10.3 cd $A^{-1}$ and 7.67% at 20 mA $cm^{-2}$, respectively. This increase in efficiency might be partially due to the differences in the effectiveness of exciton formation on dopant materials through energy transfer between the MADN host material and dopants **7** and **8** within devices **7A** and **8A**, respectively. Among dopants **1**–**14**, the degree

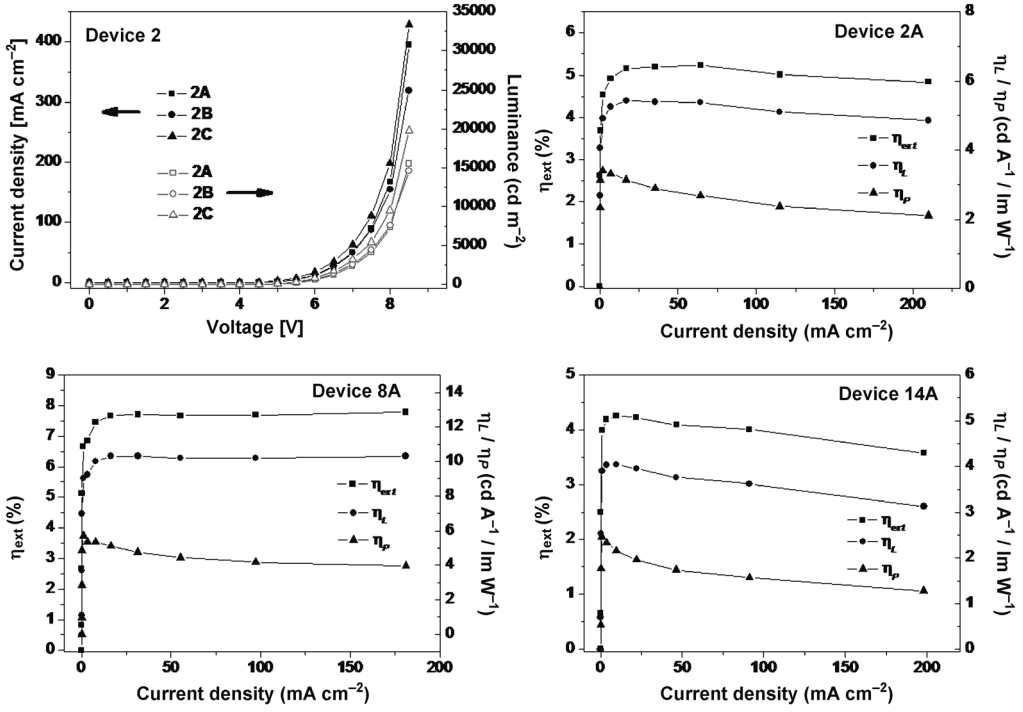


Figure 6. *I*–*V*–*L* characteristics of devices **2A**–**2C** (closed symbols: current density; open symbols: luminance) and the efficiency versus current density relationship for devices **2A**, **8A**, and **14A**.

of overlap between the absorption spectra of dopants **7** and **8** and the emission spectra of MADN host was most effective, as shown in Figure 1. These observations suggest that exciton formation on the dopant materials was most effective in devices **7A** and **8A** through energy transfer between the MADN host material and dopants **7** and **8**. Therefore, the improved efficiencies in devices **7A** and **8A** suggest that effective energy transfer between the host and dopant play an important role in the highly efficient blue OLEDs. In particular, relative to device **7A**, the EQE and luminous efficiency of device **8A** increased by 12 and 22%, respectively. The higher quantum yield of dopant **8** (0.97) than that of dopant **7** (0.81) may have contributed partially to the improved EL performance. Moreover, in device **8**, the effect of the suppression of self-quenching by the spirobifluorene moiety in dopant **8** may have partially contributed to the improved EL performance, because the EL efficiencies of device **8A** do not decrease significantly at higher doping concentrations. Interestingly, the EL efficiency of device **12A** was not high as that of devices **7A** and **8A** despite the overlap of the emission spectra of the MADN host, with the absorption spectra of dopant **12** being as effective as that of dopants **7** and **8**. Presumably, compared to compounds **7** and **8**, the higher HOMO energy level of compound **12** would facilitate the hole-trapping process in device **12A**. This would prevent effective exciton formation on the dopant through an energy-transfer process, and reduce the EL efficiency of device **12A** relative to devices **7A** and **8A**. Among devices **1A**–**14A**, devices **13A** showed the lowest EQE, with 3.20% at 20 mA cm$^{-2}$. This low efficiency might be attributed partially to the ineffective exciton formation on dopant **13** in device **13A** through the energy-transfer process because, among dopants **1**–**14**, the degree of overlap between the absorption spectra of dopant **13** and the emission spectra of the MADN host was the least effective, as shown in Figure 1. In addition, the low quantum yield of dopant **13** (0.62) might have contributed partially to the reduced EL efficiency of device **13A**. The rather improved efficiency of the device **14** is due to improved charge balance by the electron trapping by the dopant **14**. The charge trapping also affected the turn-on voltage of the device in addition to the charge-transport properties of the dopant. The turn-on voltage was defined as the voltage at 1 cd m$^{-2}$, which was different depending on the dopant materials because of the different charge-transport properties of the dopant materials and the different charge trapping caused by different HOMO and LUMO levels.

## Conclusion

Highly efficient blue fluorescent materials were developed with 2-(diphenylamino)fluoren-7-ylvinylarene emitting units and *tert*-butyl-based blocking units. Efficient, deep blue emission with an external quantum efficiency of 5.17% was obtained using a core 2-(diphenylamino)fluoren-7-ylstyrene emitting unit. Stable CIE coordinates were achieved irrespective of the doping concentrations from 5 to 15% due to the effects of the *tert*-butyl-based blocking group. The EL spectra were insensitive to the doping concentrations and high efficiency was obtained, even at high concentrations, due to the blocking group. Therefore, a blue fluorescent device with high efficiency and stable CIE coordinates can be fabricated regardless of the doping concentration by combining a highly efficient 2-(diphenylamino)fluoren-7-ylstyrene emitting unit and *tert*-butyl-based blocking groups. In addition, highly efficient sky-blue materials were developed that bore 2-(diphenylamino)fluoren-7-ylvinylarene emitting units and *tert*-butyl-based blocking units. Efficient, sky-blue emission with a quantum efficiency of 7.72% was obtained using the core 2-(diphenylamino)fluoren-7-ylvinylspirobifluorene-emitting unit. The introduction of bulky building units, such as spirobifluorene to the emitting core (**2** versus **8**), improved the current efficiency of the OLEDs by 90%. When the *tert*-butyl group and fluorine were combined and added to the diphenylaminofluorene group of compound **14**, device **14A** exhibited a deep-blue emission of 0.11, which is superior to that of device **13A** (0.15). A deep-blue device with CIE coordinates of (0.15, 0.11) that used compound **14** as a dopant in the emitting layer showed a luminous efficiency of 3.95 cd A$^{-1}$ and an external quantum efficiency of 4.23% at 20 mA cm$^{-2}$. These results clearly demonstrate the excellent properties of fluorene derivatives with suitable substituents for applications in blue-emitting materials in OLEDs.

## Experimental Section

**Synthesis and characterization**: All reactions were performed under nitrogen and the solvents were dried and distilled from the appropriate drying agents prior to use. Commercially available reagents were used without further purification unless stated otherwise. 4-Diphenylcarboxaldehyde, 4-formylphenylboronic acid, 3,5-di-*tert*-butylaniline, and 1-bromo-4-*tert*-butylbenzene were used as received from Aldrich or TCI. 7-(Diphenylamino)-9,9-diethyl-9*H*-fluorene-2-carbaldehyde,[24] 7-(diphenylamino)-2-(4-bromostyryl)-9,9-diethyl-9*H*-fluorene,[24] diethyl (4-bromobenzyl)methylphosphonate,[25] 4-bromo-2,7-di-*tert*-butyl-9,9-diethylfluorene,[26] 2-bromo-4,4′-di-*tert*-butylbiphenyl,[27] 3,7-di-*tert*-butylnaphthalenyl-1-boronic acid,[28] 3′,5′-di-*tert*-butylbiphenyl-4-carbaldehyde,[29] 7-bromo-9,9-diethylfluorene-2-carbaldehyde,[30] 7-bromospirobifluorene-2-carbaldehyde,[31] 2-(3,5-di-*tert*-butylphenyl)-4,4,5,5-tetramethyl-1,3,2-dioxaborolane,[32] 7-bromo-9,9-diphenyl-9*H*-fluorene-2-carbaldehyde,[33] 2,7-dibromo-1′,3′-dihydrospiro[9*H*-fluorene-9,2′-(2*H*)indene],[34] and 7-(diphenylamino)-9,9-diethylfluorene-2-ylmethylphosphonate[35] were prepared using previously published methods. The $^{1}$H and $^{13}$C NMR spectra were obtained using a Varian (Unity Inova 300Nb) spectrometer at 300 MHz. The FTIR spectra were acquired using a VERTEX 70 spectrometer. The low- and high-resolution mass spectra were obtained using either a Jeol JMS-AX505WA spectrometer in FAB mode, a Jeol JMS-600 spectrometer in EI mode, or a JMS-T100TD (AccuTOF-TLC) spectrometer in positive-ion mode. Elemental analysis (EA) was performed using an EA 1108 spectrometer. The UV/Vis absorption spectra were measured using a Shinco S-3100 spectrometer, and the PL spectra were measured using an Aminco–Bowman Series 2 luminescence spectrometer. The UV/Vis and PL spectra were measured in $10^{-5}$ M dilute dichloromethane solutions. The fluorescent quantum yield was determined for solutions of the compounds in dichloromethane at 293 K using BDAVBi as a reference ($\Phi = 0.86$).[8] The ionization potentials (or HOMO energy levels) of the

  

blue material thin films were determined by UV photoemission spectroscopy using a Surface Analyzer model AC-2 (Riken-Keiki AC-2). The LUMO energy levels were estimated by subtracting the bandgap energy from the HOMO energy levels. The energy gaps were determined by the on-set absorption energy based on the absorption spectra of the materials.

**Compound 1**: KO(*t*Bu) (2.40 mL, 1.0 M, 2.40 mmol) in THF was added dropwise to a mixture of 7-(diphenylamino)-9,9-diethylfluorene-2-ylmethylphosphonate (1.13 g, 2.10 mmol) and diphenylcarboxaldehyde (0.360 g, 2.00 mmol) in anhydrous THF (20.0 mL) at 0 °C under nitrogen. The reaction mixture was stirred for 15 min at 0 °C followed by 1 h at room temperature, quenched with water, extracted with ethyl acetate, and washed twice with water. The combined organic layers were dried over $MgSO_4$ and the solvent was removed under reduced pressure. The residue was purified by silica gel column chromatography using ethyl acetate/hexane (1:20 v/v) and subsequent recrystallization from $CH_2Cl_2$/MeOH to produce **1** (0.520 g, 45% yield). M.p. 214–216 °C; $^1$H NMR (300 MHz, $CDCl_3$): $\delta$ = 7.65–7.59 (m, 7H), 7.56 (d, $J$ = 8.2 Hz, 1H), 7.50 (d, $J$ = 1.3 Hz, 1H), 7.47–7.42 (m, 3H), 7.34 (t, $J$ = 7.3 Hz, 1H), 7.28–7.20 (m, 6H), 7.14–7.10 (m, 5H), 7.05 (d, $J$ = 1.0 Hz, 1H), 7.01 (t, $J$ = 7.3 Hz, 2H), 1.96 (q, $J$ = 7.2 Hz, 4H), 0.39 ppm (t, $J$ = 7.3 Hz, 6H); $^{13}$C NMR (75 MHz, $CDCl_3$): $\delta$ = 151.9, 150.7, 148.2, 147.5, 141.5, 140.9, 140.3, 136.9, 136.6, 135.8, 129.7, 129.4, 129.0, 127.6, 127.5, 127.3, 127.1, 126.2, 124.1, 123.9, 122.7, 120.8, 120.6, 119.6, 119.5, 56.3, 33.0, 8.9 ppm; FTIR (ATR): $\tilde{\nu}$ = 3029, 2969, 1586, 1487, 1468, 1334, 1299, 1267, 962, 822, 758, 696 cm$^{-1}$; MS (EI$^+$): $m/z$: 567 [$M^+$]; HRMS (EI$^+$): $m/z$ calcd for $C_{43}H_{37}N$: 567.2926 [$M^+$]; found: 567.2924; elemental analysis calcd (%) for $C_{43}H_{37}N$: C 90.96, H 6.57, N 2.47; found: C 90.91, H 6.59, N 2.45.

**Compound 2**: Yield: 0.420 g, 67%; m.p. 200–202 °C; $^1$H NMR (300 MHz, $CDCl_3$): $\delta$ = 7.65–7.59 (m, 5H), 7.56 (d, $J$ = 8.2 Hz, 1H), 7.51 (d, $J$ = 1.2 Hz, 1H), 7.48–7.44 (m, 4H), 7.23 (m, 4H), 7.21 (d, $J$ = 2.8 Hz, 2H), 7.14–7.10 (m, 5H), 7.05 (d, $J$ = 2.1 Hz, 1H), 7.01 (t, $J$ = 7.2 Hz, 2H), 1.96 (q, $J$ = 7.4 Hz, 4H), 1.40 (s, 18H), 0.39 ppm (t, $J$ = 7.3 Hz, 6H); $^{13}$C NMR (75 MHz, $CDCl_3$): $\delta$ = 151.9, 151.4, 150.7, 148.3, 147.5, 141.6, 141.4, 140.4, 136.7, 136.6, 135.9, 129.4, 127.9, 127.5, 127.0, 126.2, 124.1, 123.9, 122.7, 121.7, 121.6, 120.8, 120.6, 119.6, 119.5, 56.3, 35.2, 33.0, 31.8, 8.9 ppm; FTIR (ATR): $\tilde{\nu}$ = 3026, 2965, 2869, 1593, 1492, 1468, 1330, 1321, 1307, 1276, 1246, 963, 877, 857, 819, 757, 743, 694, 663 cm$^{-1}$; MS (EI$^+$): $m/z$: 679 [$M^+$]; HRMS (EI$^+$): $m/z$ calcd for $C_{51}H_{53}N$: 679.4178 [$M^+$]; found: 679.4182; elemental analysis calcd (%) for $C_{51}H_{53}N$: C 90.08, H 7.86, N 2.06; found: C 90.12, H 7.84, N 2.05.

**Compound 3**: Toluene (10.0 mL), EtOH (3.00 mL), and a $K_2CO_3$ solution (3.4 mL of 2.0 M) were added stepwise to a 30.0 mL, two-necked, round-bottomed flask that contained 7-(diphenylamino)-2-(4-bromostyryl)-9,9-diethyl-9*H*-fluorene (0.390 g, 0.680 mmol), [3,7-bis(1,1-dimethylethyl)-1-naphthalenyl]boronic acid (0.300 g, 0.820 mmol), and tetrakis(triphenylphosphine)palladium(0) (31.0 mg, 0.0270 mmol). The reaction mixture was heated under reflux at 120 °C for 3 h. The mixture was then extracted with ethyl acetate and washed with water. The combined organic layers were dried with anhydrous $MgSO_4$, filtered, and the solvent was removed by evaporation to dryness. The residue was purified by silica gel column chromatography using dichloromethane/hexane (1:3 v/v) to produce compound **3** (0.350 g 73% yield). M.p. 226–228 °C; $^1$H NMR (300 MHz, $CDCl_3$): $\delta$ = 7.90 (d, $J$ = 1.6 Hz, 1H), 7.83 (d, $J$ = 8.7 Hz, 1H), 7.75 (d, $J$ = 1.6 Hz, 1H), 7.68 (d, $J$ = 8.2 Hz, 2H), 7.64–7.50 (m, 8H), 7.29–7.23 (m, 6H), 7.18–7.10 (m, 5H), 7.06 (d, $J$ = 2.1 Hz, 1H), 7.01 (t, $J$ = 6.9 Hz, 2H), 1.97 (q, $J$ = 7.4 Hz, 4H), 1.44 (s, 9H), 1.32 (s, 9H), 0.40 ppm (t, $J$ = 7.0 Hz, 6H); $^{13}$C NMR (75 MHz, $CDCl_3$): $\delta$ = 151.9, 150.7, 148.4, 148.3 147.7, 147.5, 141.5, 140.7, 139.7, 136.7, 136.6, 135.9, 132.3, 130.7, 129.7, 129.6, 129.4, 128.9, 128.2, 127.8, 127.6, 126.6, 126.5, 126.2, 124.7, 124.1, 123.9, 122.7, 122.5, 120.8, 120.6, 119.6, 56.3, 35.2, 35.1, 33.0, 31.6, 31.5, 8.9 ppm; FTIR (ATR): $\tilde{\nu}$ = 3029, 2964, 1591, 1493, 1466, 1332, 1278, 962, 881, 823, 811, 752, 695 cm$^{-1}$; MS (FAB$^+$): $m/z$: 729 [$M^+$]; HRMS (FAB$^+$): $m/z$ calcd for $C_{55}H_{55}N$: 729.4335 [$M^+$]; found: 729.4342; elemental analysis calcd (%) for $C_{55}H_{55}N$: C 90.49, H 7.56, N 1.92; found: C 90.41, H 7.55, N 1.95.

**Compound 4**: Yield: 0.420 g, 46%; m.p. 218–220 °C; $^1$H NMR (300 MHz, $CDCl_3$): $\delta$ = 7.64 (t, $J$ = 8.3 Hz, 4H), 7.57 (d, $J$ = 8.1 Hz, 2H), 7.52 (d, $J$ = 8.5 Hz, 5H), 7.31–7.23 (m, 10H), 7.18–7.12 (m, 8H), 7.07–6.99 (m, 6H), 6.93 (d, $J$ = 8.2 Hz, 2H), 2.06–1.94 (m, 4H), 1.39 (s, 9H), 1.31 (s, 9H), 0.41 ppm (t, $J$ = 7.0 Hz, 6H); $^{13}$C NMR (75 MHz, $CDCl_3$): $\delta$ = 151.9, 151.0, 150.7, 150.6, 149.7, 149.6, 148.3, 147.4, 141.4, 139.0, 136.7, 136.3, 136.0, 135.9, 130.0, 129.5, 129.4, 127.7, 126.5, 126.2, 125.8, 124.1, 123.9, 123.4, 122.7, 121.8, 120.8, 120.6, 119.7, 119.6, 119.5, 118.9, 56.3, 55.5, 35.1, 35.0, 33.2, 33.0, 31.9, 31.8, 8.9, 8.8 ppm; FTIR (ATR): $\tilde{\nu}$ = 3029, 2961, 1594, 1511, 1494, 1361, 1334, 1278, 1231, 1216, 1202, 957, 876, 823, 752, 696 cm$^{-1}$; MS (FAB$^+$): $m/z$: 823 [$M^+$]; HRMS (FAB$^+$): $m/z$ calcd for $C_{62}H_{65}N$: 823.5117 [$M^+$]; found: 823.5117; elemental analysis calcd (%) for $C_{62}H_{65}N$: C 90.35, H 7.95, N 1.70; found: C 90.41, H 7.93, N 1.67.

**Compound 5**: Yield: 0.430 g, 47%; m.p. 110–112 °C; $^1$H NMR (300 MHz, $CDCl_3$): $\delta$ = 7.58 (d, $J$ = 7.8 Hz, 1H), 7.55 (d, $J$ = 8.2 Hz, 1H), 7.47–7.37 (m, 7H), 7.29–7.22 (m, 6H), 7.18–7.08 (m, 11H), 7.04 (d, $J$ = 1.8 Hz, 1H), 7.00 (t, $J$ = 7.3 Hz, 2H), 2.00–1.89 (m, 4H), 1.40 (s, 9H), 1.30 (s, 9H), 0.37 ppm (t, $J$ = 7.3 Hz, 6H); $^{13}$C NMR (75 MHz, $CDCl_3$): $\delta$ = 151.8, 150.6, 150.4, 149.4, 148.2, 147.4, 141.7, 141.4, 139.9, 138.5, 137.8, 136.6, 135.9, 135.8, 130.7, 130.5, 130.1, 129.7, 129.4, 129.2, 127.8, 127.6, 126.2, 125.0, 124.8, 124.1, 123.9, 122.7, 120.7, 120.6, 119.6, 119.5, 56.3, 34.9, 34.7, 33.0, 31.7, 31.6, 8.8 ppm; FTIR (ATR): $\tilde{\nu}$ = 3028, 2963, 1586, 1487, 1466, 1362, 1278, 1228, 1204, 960, 824, 756, 746, 695 cm$^{-1}$; MS (FAB$^+$): $m/z$: 755 [$M^+$]; HRMS (FAB$^+$): $m/z$ calcd for $C_{57}H_{57}N$: 755.4491 [$M^+$]; found: 755.4479; elemental analysis calcd (%) for $C_{57}H_{57}N$: C 90.55, H 7.60, N 1.85; found: C 90.61, H 7.58, N 1.82.

**Compound 6**: Yield: 0.468 g, 27%; m.p. 132–134 °C; $^1$H NMR (300 MHz, $CDCl_3$): $\delta$ = 7.69–7.62 (m, 5H), 7.60 (s, 1H), 7.57 (d, $J$ = 8.2 Hz, 2H), 7.53 (s, 1H), 7.50 (s, 6H), 7.30 (s, 2H), 7.24–7.23 (m, 2H), 7.13–7.11 (m, 5H), 7.05–6.99 (m, 3H), 2.05–1.89 (m, 4H), 1.41 (s, 36H), 0.39 ppm (t, $J$ = 7.2 Hz, 6H); $^{13}$C NMR (75 MHz, $CDCl_3$): $\delta$ = 151.8, 151.5, 150.7, 148.2, 147.5, 143.7, 141.5, 141.1, 138.5, 136.6, 135.8, 130.2, 129.4, 127.9, 126.6, 126.3, 124.6, 124.1, 123.9, 122.7, 122.2, 121.9, 120.8, 120.6, 119.6, 119.5, 56.3, 35.3, 33.0, 31.8, 8.8 ppm; FTIR (ATR): $\tilde{\nu}$ = 2963, 2870, 1588, 1494, 1467, 1278, 1249, 867, 752, 713, 697 cm$^{-1}$; MS (FAB$^+$): $m/z$: 868 [$M^+$]; HRMS (FAB$^+$): $m/z$ calcd for $C_{65}H_{73}N$: 867.5743 [$M^+$]; found: 867.5738; elemental analysis calcd (%) for $C_{65}H_{73}N$: C 89.91, H 8.47, N 1.61; found: C 89.78, H 8.39, N 1.57.

**Compound 7**: Yield: 0.450 g, 40%; m.p. 246–248 °C; $^1$H NMR (300 MHz, $CDCl_3$): $\delta$ = 7.76–7.70 (m, 3H), 7.62–7.46 (m, 12H), 7.28–7.23 (m, 4H), 7.13 (d, $J$ = 7.9 Hz, 4H), 7.05–6.98 (m, 4H), 2.15–1.91 (m, 8H), 1.41 (s, 18H), 0.41–0.33 ppm (m, 12H); $^{13}$C NMR (75 MHz, $CDCl_3$): $\delta$ = 151.8, 151.4, 151.0, 150.6, 148.3, 147.4, 141.7, 141.4, 141.3, 141.2, 140.5, 136.7, 136.1, 129.4, 128.8, 128.5, 126.7, 126.1, 126.0, 124.1, 123.9, 122.7, 122.1, 121.9, 121.6, 120.9, 120.8, 120.6, 120.1, 1120.0, 119.6, 119.6, 56.4, 56.3, 35.3, 33.1, 33.0, 31.8, 8.9, 8.8 ppm; FTIR (ATR): $\tilde{\nu}$ = 2967, 2876, 1592, 1492, 1469, 1324, 1273, 1216, 1203, 964, 873, 817, 745, 696, 660 cm$^{-1}$; MS (FAB$^+$): $m/z$: 823 [$M^+$]; HRMS (FAB$^+$): $m/z$ calcd for $C_{62}H_{65}N$: 823.5117 [$M^+$]; found: 823.5131; elemental analysis calcd (%) for $C_{62}H_{65}N$: C 90.35, H 7.95, N 1.70; found: C 90.30, H 7.98, N 1.67.

**Compound 8**: Yield: 0.370 g, 45%; m.p. 254–256 °C; $^1$H NMR (300 MHz, $CDCl_3$): $\delta$ = 7.89 (d, $J$ = 6.9 Hz, 2H), 7.85 (d, $J$ = 8.1 Hz, 1H), 7.61–7.50 (m, 4H), 7.41–7.31 (m, 5H), 7.26–7.20 (m, 6H), 7.16–7.06 (m, 8H), 7.01–6.97 (m, 5H), 6.87 (s, 2H), 6.84 (d, $J$ = 7.6 Hz, 2H), 1.90–1.85 (m, 4H), 1.29 (s, 18H), 0.31 ppm (t, $J$ = 7.2 Hz, 6H); $^{13}$C NMR (75 MHz, $CDCl_3$): $\delta$ = 151.8, 151.2, 150.5, 150.1, 149.7, 149.0, 148.2, 147.4, 142.6, 142.1, 141.3, 141.1, 140.9, 140.8, 137.6, 136.7, 135.8, 129.4, 129.1, 128.2, 128.0, 127.7, 126.6, 126.0, 124.6, 124.4, 124.1, 123.9, 123.3, 122.7, 122.0, 121.9, 121.6, 120.7, 120.5, 120.4, 120.3, 120.2, 119.6, 119.4, 76.8, 66.3, 56.2, 35.1, 32.9, 31.7, 8.8 ppm; FTIR (ATR): $\tilde{\nu}$ = 3025, 2965, 2873, 1594, 1493, 1466, 1447, 1362, 1278, 1230, 1216, 1205, 961, 872, 816, 752, 696, 660, 639 cm$^{-1}$; MS (FAB$^+$): $m/z$: 917 [$M^+$]; HRMS (FAB$^+$): $m/z$ calcd for $C_{70}H_{63}N$: 917.4961 [$M^+$]; found: 917.4961; elemental analysis calcd (%) for $C_{70}H_{63}N$: C 91.56, H 6.92, N 1.53; found: C 91.62, H 6.89, N 1.49.

**Compound 9**: Compound **21** (0.400 g, 0.870 mmol), diphenylamine (0.203 g, 1.00 mmol), [$Pd_2$(dba)$_3$] (dba = dibenzylideneacetone; 40.0 mg, 43.0 μmol), sodium *tert*-butoxide (0.167 g, 1.74 mmol), and tri-*tert*-butylphosphine (24.0 mg, 80.0 μmol) were mixed in a two-necked, round-bottomed flask that contained toluene (30.0 mL). The mixture was heated under reflux for 4 h under argon. Water was added to the mixture and

  

the solution was extracted with toluene. The combined organic extracts were dried ($MgSO_4$) and concentrated. Column chromatography on silica gel (hexane/dichloromethane, 5:1) afforded compound **9** (0.250 g, 55% yield). M.p. 138–140°C; $^1$H NMR (300 MHz, $CDCl_3$): $\delta$=7.77 (d, $J$=7.4 Hz, 2H), 7.70 (d, $J$=7.9 Hz, 1H), 7.65 (d, $J$=8.2 Hz, 1H), 7.52–7.49 (m, 3H), 7.43–7.40 (m, 5H), 7.33 (t, $J$=7.3 Hz, 1H), 7.18–7.06 (m, 7H), 7.01–6.92 (m, 8H), 6.88–6.83 (m, 4H), 6.54 (s, 1H), 1.36 ppm (s, 18H); $^{13}$C NMR (75 MHz, $CDCl_3$): $\delta$=151.4, 150.8, 149.6, 149.0, 147.9, 147.8, 142.0, 141.6, 141.5, 140.4, 136.7, 136.6, 136.4, 129.3, 128.7, 128.1, 128.0, 127.9, 127.0, 124.3, 124.1, 122.9, 122.0, 121.7, 120.9, 120.4, 120.1, 119.9, 66.1, 35.3, 31.8 ppm; FTIR (ATR): $\tilde{\nu}$=2961, 1594, 1482, 1467, 1303, 1270, 820, 744, 698 cm$^{-1}$; MS (FAB$^+$): $m/z$: 773 [$M^+$]; HRMS-TOF: $m/z$ calcd for $C_{56}H_{52}N$: 774.4100 [$M^+$+H]; found: 774.4115; elemental analysis calcd (%) for $C_{56}H_{52}N$: C 91.55, H 6.64, N 1.81; found: C 91.50, H 6.65, N 1.79.

**Compound 10**: Yield: 0.260 g, 76%; m.p. 140–142°C; $^1$H NMR (300 MHz, $CDCl_3$): $\delta$=7.66 (d, $J$=7.9 Hz, 1H), 7.59–7.53 (m, 6H), 7.50 (s, 2H), 7.44 (s, 3H), 7.22–7.18 (m, 12H), 7.12–7.05 (m, 7H), 7.03–6.06 (m, 4H), 1.39 ppm (s, 18H); $^{13}$C NMR (75 MHz, $CDCl_3$): $\delta$=153.2, 151.6, 151.4, 147.8, 145.0, 141.7, 140.4, 140.0, 136.4, 136.3, 134.5, 129.4, 129.1, 128.5, 128.4, 128.3, 127.8, 126.9, 126.8, 126.4, 124.6, 124.5, 123.3, 123.1, 121.8, 121.7, 120.9, 120.0, 68.2, 56.6, 35.2, 31.8 ppm; FTIR (ATR): $\tilde{\nu}$=3030, 2963, 1591, 1491, 1468, 1282, 963, 7523, 697 cm$^{-1}$; MS (FAB$^+$): $m/z$: 775 [$M^+$]; HRMS (FAB$^+$): $m/z$ calcd for $C_{59}H_{53}N$: 775.4178 [$M^+$]; found: 775.4177; elemental analysis calcd (%) for $C_{59}H_{53}N$: C 91.31, H 6.88, N 1.80; found: C 91.35, H 6.83, N 1.79.

**Compound 11**: Yield: 0.220 g, 56%; m.p. 122–124°C; $^1$H NMR (300 MHz, $CDCl_3$): $\delta$=7.60 (t, $J$=7.3 Hz, 2H), 7.52 (t, $J$=7.9 Hz, 5H), 7.43 (s, 3H), 7.27–7.20 (m, 8H), 7.11–7.08 (m, 6H), 7.05–6.95 (m, 5H), 3.44 (d, $J$=16 Hz, 2H), 3.33 (d, $J$=16 Hz, 2H), 1.38 ppm (s, 18H); $^{13}$C NMR (75 MHz, $CDCl_3$): $\delta$=154.0, 153.8, 151.4, 148.0, 147.9, 142.8, 141.6, 140.4, 139.1, 136.5, 136.2, 134.4, 129.5, 129.1, 127.9, 127.6, 127.1, 126.9, 126.1, 124.9, 124.5, 123.3, 123.1, 121.7, 120.6, 120.3, 119.6, 118.3, 57.3, 45.8, 35.2, 31.8 ppm; FTIR (ATR): $\tilde{\nu}$=3028, 2963, 1589, 1490, 1467, 1297, 963, 898, 750, 696 cm$^{-1}$; MS (FAB$^+$): $m/z$: 725 [$M^+$]; HRMS (FAB$^+$): $m/z$ calcd for $C_{55}H_{51}N$: 725.4022 [$M^+$]; found: 725.4016; elemental analysis calcd (%) for $C_{55}H_{51}N$: C 90.99, H 7.08, N 1.93; found: C 90.91, H 7.10, N 1.91.

**Compound 12**: Yield: 0.432 g, 53%; m.p. 120–122°C; $^1$H NMR (300 MHz, $CDCl_3$): $\delta$=7.61 (s, 4H), 7.54 (d, $J$=8.2 Hz, 1H), 7.50–7.44 (m, 7H), 7.26–7.23 (m, 4H), 7.22 (s, 1H), 7.13–7.06 (m, 3H), 6.97 (s, 2H), 2.04–1.89 (m, 4H), 1.40 (s, 18H), 1.33 (s, 9H), 1.25 (s, 18H), 0.37 ppm (t, $J$=7.3 Hz, 6H); $^{13}$C NMR (75 MHz, $CDCl_3$): $\delta$=151.7, 151.4, 141.6, 140.4, 136.7, 129.5, 127.9, 127.2, 126.9, 126.0, 123.4, 121.7, 119.4, 118.7, 116.6, 56.3, 35.2, 35.1, 34.5, 33.1, 31.8, 31.7, 31.6, 8.9 ppm; FTIR (ATR): $\tilde{\nu}$=2963, 2868, 1593, 1512, 1466, 1248, 822, 710 cm$^{-1}$; MS (FAB$^+$): $m/z$: 847 [$M^+$]; HRMS-TOF: $m/z$ calcd for $C_{68}H_{78}N$: 848.6134 [$M^+$+H]; found: 848.6127; elemental analysis calcd (%) for $C_{68}H_{78}N$: C 89.20, H 9.15, N 1.65; found: C 89.15, H 9.18, N 1.62.

**Compound 13**: Yield: 0.328 g, 68%; m.p. 190–192°C; $^1$H NMR (300 MHz, $CDCl_3$): $\delta$=7.61 (s, 4H), 7.58 (s, 1H), 7.56 (d, $J$=8.1 Hz, 1H), 7.49 (d, $J$=7.8 Hz, 1H), 7.46–7.44 (m, 4H), 7.28–7.24 (m, 2H), 7.23 (s, 1H), 7.21–7.19 (m, 2H), 7.03–6.99 (m, 4H), 6.98–6.95 (m, 1H), 6.88 (d, $J$=8.1 Hz, 2H), 1.99–1.91 (m, 4H), 1.38 (s, 18H), 0.36 ppm (t, $J$=7.2 Hz, 6H); $^{13}$C NMR (75 MHz, $CDCl_3$): $\delta$=160.0 (dd, $J$(F,C)=11.0, 247.3 Hz), 158.4 (dd, $J$(F,C)=12.2, 254.3 Hz), 151.7, 151.2, 150.4, 147.4, 146.5, 141.4, 141.2, 140.2, 136.4, 136.3, 135.7, 131.1 (dd, $J$(F,C)=3.9, 10.5 Hz), 129.9 (d, $J$(F,C)=9.4 Hz), 129.2, 127.7, 127.3, 126.8, 125.9, 122.2, 121.7, 121.5, 120.5, 120.4, 119.3, 117.5, 112.0 (dd, $J$(F,C)=3.8, 22.4 Hz), 105.5 (dd, $J$(F,C)=23.8, 26 Hz), 56.1, 35.0, 32.8, 31.6, 8.6 ppm; FTIR (ATR): $\tilde{\nu}$=2964, 1595, 1503, 1467, 1264, 1144, 944, 853, 821, 741, 711, 695 cm$^{-1}$; MS (FAB$^+$): $m/z$: 715 [$M^+$]; HRMS (FAB$^+$): $m/z$ calcd for $C_{51}H_{51}F_2N$: 715.3990 [$M^+$]; found: 715.3985; elemental analysis calcd (%) for $C_{51}H_{51}F_2N$: C 85.56, H 7.18, N 1.96; found: C 85.12, H 7.02, N 1.91.

**Compound 14**: Yield: 0.200 g, 79%; m.p. 212–214°C; $^1$H NMR (300 MHz, $CDCl_3$): $\delta$=7.61 (s, 4H), 7.58 (s, 1H), 7.53 (d, $J$=8.2 Hz, 2H), 7.48 (d, $J$=8.2 Hz, 1H), 7.45–7.43 (m, 4H), 7.22 (d, $J$=2.0 Hz, 1H), 7.07 (t, $J$=1.6 Hz, 1H), 6.88–6.83 (m, 5H), 2.08–1.85 (m, 4H), 1.39 (s, 18H), 1.25 (s, 18H), 0.36 ppm (t, $J$=7.2 Hz, 6H); $^{13}$C NMR (75 MHz, $CDCl_3$): $\delta$=160.7 (dd, $J$(F,C)=11.0, 257.6 Hz), 157.4 (dd, $J$(F,C)=11.8, 242.1 Hz), 151.6, 151.3, 151.2, 150.1, 146.9, 146.5, 141.4, 141.3, 140.2, 136.4, 135.7, 135.4, 131.4 (d, $J$(F,C)=6.6 Hz), 130.0 (d, $J$(F,C)=9.4 Hz), 129.2, 127.7, 127.1, 126.7, 125.9, 121.5, 120.8, 120.5, 120.2, 119.2, 116.5, 111.9 (d, $J$(F,C)=22.1 Hz), 105.3 (dd, $J$(F,C)=23.8, 26.0 Hz), 56.1, 35.1, 34.9, 32.9, 31.6, 31.4, 8.63 ppm; FTIR (ATR): $\tilde{\nu}$=2963, 1593, 1505, 1465, 1428, 1141, 859, 823, 711 cm$^{-1}$; MS (FAB$^+$): $m/z$: 828 [$M^+$]; HRMS (FAB$^+$): $m/z$ calcd for $C_{59}H_{67}F_2N$: 827.5242 [$M^+$]; found: 827.5238; elemental analysis calcd (%) for $C_{59}H_{67}F_2N$: C 85.57, H 8.15, N 1.69; found: C 85.07, H 8.01, N 1.61.

**Device fabrication and characterization**: The device configuration of the blue devices was indium–tin oxide (ITO, 150 nm)/*N,N′*-diphenyl-*N,N′*-bis-[4-(phenyl-*m*-tolylamino)phenyl]biphenyl-4,4′-diamine (DNTPD, 60 nm)/*N,N′*-di(1-naphthyl)-*N,N′*-diphenylbenzidine (NPB, 30 nm)/MADN:dopants (30 nm)/tris(8-hydroxyquinoline) aluminium ($Alq_3$, 20 nm)/LiF (1.0 nm)/Al (200 nm). DNTPD and NPB were hole-injection and hole-transport materials, respectively. $Alq_3$ was used as an electron-transport layer and LiF/Al as a cathode. All organic materials except for dopants were deposited at a deposition rate of 1 Å s$^{-1}$. Current ($I$)/voltage ($V$)/luminance ($L$) characteristics and electroluminescence (EL) spectra of the devices were measured using a Keithley 2400 source measurement unit and CS 1000A spectrophotometer.

## Acknowledgements

This research was supported by Basic Science Research Program through the National Research Foundation of Korea (NRF) funded by the Ministry of Education, Science and Technology (20100007370). J.Y. Lee acknowledges the NRF (grant no. 2010-0001630) funded by MEST, Republic of Korea. J.Y. Lee acknowledges the financial support from the Fundamental R&D Program for Core Technology of Materials (grant no. M2009010025) funded by the MKE, GRRC program of Gyeonggi Province (GRRC Dankook2010-B01: Materials Development for High-Efficiency Solid-State Lighting) and Development of Core Technologies for Organic Materials Applicable to OLED Lighting with High Color Rendering Index by MKE.

[1] C. W. Tang, S. A. VanSlyke, *Appl. Phys. Lett.* **1987**, *51*, 913.
[2] C. W. Tang, S. A. VanSlyke, *Appl. Phys. Lett.* **1989**, *65*, 3610.
[3] J. M. Shi, C. W. Tang, *Appl. Phys. Lett.* **1997**, *70*, 1665.
[4] P. E. Burrows, S. R. Forrest, *Appl. Phys. Lett.* **2000**, *76*, 2493.
[5] S. W. Wen, M. T. Lee, C. H. Chen, *J. Disp. Technol.* **2005**, *1*, 1.
[6] J. Shi, C. W. Tang, *Appl. Phys. Lett.* **2002**, *80*, 3201.
[7] C. Hosokawa, H. Higashi, H. Nakamura, T. Kusumoto, *Appl. Phys. Lett.* **1995**, *67*, 3853.
[8] C. L. Li, S. J. Shieh, S. C. Lin, R. S. Liu, *Org. Lett.* **2003**, *5*, 1131.
[9] J. M. Kauffman, G. J. Moyna, *J. Org. Chem.* **2003**, *68*, 839.
[10] M. T. Lee, C. H. Liao, C. H. Tsai, C. H. Chen, *Adv. Mater.* **2005**, *17*, 2493.
[11] Z. Q. Gao, B. X. Mi, C. H. Chen, K. W. Cheah, K. Y. Cheng, W. S. Wen, *Appl. Phys. Lett.* **2007**, *90*, 123506.
[12] H. Reisch, U. Wiester, U. Scherf, N. Tuytuylkov, *Macromolecules* **1996**, *29*, 8204.
[13] M. Ranger, D. Rondeau, M. Leclerc, *Macromolecules* **1997**, *30*, 7686.
[14] S. Inaoka, R. Advincula, *Macromolecules* **2002**, *35*, 2426.
[15] D. Marsitzky, J. C. Scott, J. P. Chen, V. Y. Lee, R. D. Miller, S. Setayesh, K. Muellen, *Adv. Mater.* **2001**, *13*, 1096.
[16] Y. H. Kim, D. C. Shin, S. H. Kim, C. H. Ko, H. S. Yu, Y. S. Chae, S. K. Kwon, *Adv. Mater.* **2001**, *13*, 1690.
[17] J. Salbeck, N. Yu, J. Bauer, F. Weissortel, H. Bestgen, *Synth. Met.* **1997**, *91*, 209.
[18] W. L. Yu, J. Pei, W. A. Huang, A. Heeger, *J. Adv. Mater.* **2000**, *12*, 828.

  

[19] R. Wu, J. S. Schumm, D. L. Pearson, J. M. Tour, *J. Org. Chem.* **1996**, *61*, 6906.
[20] M. J. Plater, T. Jackson, *Tetrahedron* **2003**, *59*, 4673.
[21] J. F. Hartwig, *Angew. Chem.* **1998**, *110*, 2154; *Chem. Int. Ed.* **1998**, *37*, 2046.
[22] Gaussian 03, Revision B05, M. J. Frisch, G. W. Trucks, H. B. Schlegel, G. E. Scuseria, M. A. Robb, J. R. Cheeseman, J. A. Montgomery, Jr., T. Vreven, K. N. Kudin, J. C. Burant, J. M. Millam, S. S. Iyengar, J. Tomasi, V. Barone, B. Mennucci, M. Cossi, G. Scalmani, N. Rega, G. A. Petersson, H. Nakatsuji, M. Hada, M. Ehara, K. Toyota, R. Fukuda, J. Hasegawa, M. Ishida, T. Nakajima, Y. Honda, O. Kitao, H. Nakai, M. Klene, X. Li, J. E. Knox, H. P. Hratchian, J. B. Cross, C. Adamo, J. Jaramillo, R. Gomperts, R. E. Stratmann, O. Yazyev, A. J. Austin, R. Cammi, C. Pomelli, J. W. Ochterski, P. Y. Ayala, K. Morokuma, G. A. Voth, P. Salvador, J. J. Dannenberg, V. G. Zakrzewski, S. Dapprich, A. D. Daniels, M. C. Strain, O. Farkas, D. K. Malick, A. D. Rabuck, K. Raghavachari, J. B. Foresman, J. V. Ortiz, Q. Cui, A. G. Baboul, S. Clifford, J. Cioslowski, B. B. Stefanov, G. Liu, A. Liashenko, P. Piskorz, I. Komaromi, R. L. Martin, D. J. Fox, T. Keith, M. A. Al-Laham, C. Y. Peng, A. Nanayakkara, M. Challacombe, P. M. W. Gill, B. Johnson, W. Chen, M. W. Wong, C. Gonzalez, J. A. Pople, Gaussian, Inc., Pittsburgh, PA **2003**.
[23] M. Ho, Y. Wu, S. Wen, T. Chen, C. H. Chen, *Appl. Phys. Lett.* **2007**, *91*, 083515.
[24] K. H. Lee, Y. S. Kwon, L. K. Kang, G. Y. Kim, J. H. Seo, Y. K. Kim, S. S. Yoon, *Synth. Met.* **2009**, *159*, 2603.
[25] L. Viau, O. Maury, H. L. Bozec, *Tetrahedron Lett.* **2004**, *45*, 125.
[26] S. Kajigaeshi, T. Kadowaki, A. Nishida, S. Fujisaki, *Bull. Chem. Soc. Jpn.* **1986**, *59*, 97.
[27] M. Tashiro, T. Yamato, *J. Org. Chem.* **1979**, *44*, 3037.
[28] U. Fahnenstich, K. H. Koch, K. Muellen, *Macromol. Chem. Rapid. Commun.* **1989**, *10*, 563.
[29] S. Mikami, K. Sugiura, Y. Sakata, *Chem. Lett.* **1997**, 833.
[30] R. Kannan, G. S. He, L. Yuan, F. Xu, P. N. Prasad, A. G. Dombroskie, B. A. Reinhardt, J. W. Baur, R. A. Vaia, L. S. Tan, *Chem. Mater.* **2001**, *13*, 1896.
[31] C. L. Chiang, M. F. Wu, D. C. Dai, Y. S. Wen, J. K. Wang, C. T. Chen, *Adv. Funct. Mater.* **2005**, *15*, 231.
[32] A. D. Finke, J. S. Moore, *Org. Lett.* **2008**, *10*, 4851.
[33] I. W. Choi, C. S. Kim, H. N. Shin, M. A. Lee, H. S. Shin, M. Y. Kwak, N. K. Kim, B. O. Kim, S. M. Kim, PCT Int. Appl. WO 2007086701A1, **2007**.
[34] I. W. Choi, C. S. Kim, H. J. Kwon, Y. J. Cho, B. O. Kim, S. M. Kim, S. S. Yoon, PCT Int. Appl. WO 2009066815A1, **2009**.
[35] K. H. Lee, L. K. Kang, J. Y. Lee, S. Kang, S. O. Jeon, K. S. Yook, J. Y. Lee, S. S. Yoon, *Adv. Funct. Mater.* **2010**, *20*, 1345.

Received: January 27, 2011
Revised: July 26, 2011
Published online: September 28, 2011

  